ADVANCED FUNCTIONAL MATERIALS
www.afm-journal.de

www.MaterialsViews.com

Temperature-Resolved Local and Macroscopic Charge Carrier Transport in Thin P3HT Layers

By *Patrick Pingel, Achmad Zen, Ruben D. Abellón, Ferdinand C. Grozema, Laurens D.A. Siebbeles,* and *Dieter Neher**

Dedicated to the 70th birthday of Prof. Dr. Gerhard Wegner.

Previous investigations of the field-effect mobility in poly(3-hexylthiophene) (P3HT) layers revealed a strong dependence on molecular weight (MW), which was shown to be closely related to layer morphology. Here, charge carrier mobilities of two P3HT MW fractions (medium-MW: $M_n = 7\,200$ g mol^{-1}; high-MW: $M_n = 27\,000$ g mol^{-1}) are probed as a function of temperature at a local and a macroscopic length scale, using pulse-radiolysis time-resolved microwave conductivity (PR-TRMC) and organic field-effect transistor measurements, respectively. In contrast to the macroscopic transport properties, the local intra-grain mobility depends only weakly on MW (being in the order of 10^{-2} cm^2 V^{-1} s^{-1}) and being thermally activated below the melting temperature for both fractions. The striking differences of charge transport at both length scales are related to the heterogeneity of the layer morphology. The quantitative analysis of temperature-dependent UV/Vis absorption spectra according to a model of F. C. Spano reveals that a substantial amount of disordered material is present in these P3HT layers. Moreover, the analysis predicts that aggregates in medium-MW P3HT undergo a "pre-melting" significantly below the actual melting temperature. The results suggest that macroscopic charge transport in samples of short-chain P3HT is strongly inhibited by the presence of disordered domains, while in high-MW P3HT the low-mobility disordered zones are bridged via inter-crystalline molecular connections.

1. Introduction

Organic electronics are expected to play a major role in the future markets, making research in this field of great interest for science and industry.[1] Solution-processable organic macromolecules, e.g., poly(3-hexylthiophene) (P3HT), are of considerable interest for the realization of low-cost electronic devices.[2–4] For many electronic applications of organic thin films, the charge carrier transport inside the organic layer, i.e., the hopping of charges in an electric field through the arrangement of innumerous molecules, determines the functionality and device performance. It is now well established that the charge carrier mobility in polymer-based devices depends critically on the chemical and electronic structure of the individual molecules as well as on the morphology of the active layer.[5–17]

A strong correlation between the field-effect mobility and the molecular weight (MW) has been observed for P3HT and related polymers. In general, the field-effect mobility was seen to significantly increase by four orders of magnitude, typically from 10^{-6} to 10^{-2} cm^2 V^{-1} s^{-1}, with an increase in the molecular weight from ~3 000 g mol^{-1} to 30 000 g mol^{-1}.[10,11,15,17] This finding stimulated detailed studies related to the morphology of the layers made from different molecular weight P3HT.[5,9–11,15–23] Kline et al. showed in their original work that low molecular weight P3HT layers appear to be more crystalline in atomic force microscopy (AFM) and X-ray investigations than their higher molecular weight counterparts.[10] In particular, the AFM images suggested the formation of rod-like nanocrystallites in low molecular weight samples. The trapping of charges at the grain boundaries between such crystals was proposed to be the cause of the poor field-effect mobility in these samples. In a later study, the same authors pointed out that long polymer chains might bridge the ordered domains in high molecular weight P3HT.[11] In 2006, Kline et al. reported a high mobility in low molecular weight P3HT prepared on a Si/SiO_2 substrate that was treated with

[*] Prof. D. Neher, P. Pingel
Institute of Physics and Astronomy
University of Potsdam
Karl-Liebknecht-Straße 24-25
14476 Potsdam (Germany)
E-mail: neher@uni-potsdam.de
Dr. A. Zen
Robert Bosch Pte Ltd
Research and Technology Center Asia Pacific
11 Bishan Street 21
Singapore 537943 (Singapore)
R. D. Abellón, Dr. F. C. Grozema, Prof. L. D. A. Siebbeles
Opto-Electronic Materials Section
Department of Chemical Engineering
Delft University of Technology
Julianalaan 136, 2628 BL Delft (The Netherlands)

DOI: 10.1002/adfm.200902273

octadecyltrichlorosilane (OTS).[21] Based on the results of X-ray rocking-curve measurements, the authors concluded that low molecular weight P3HT on an OTS-treated substrate exhibits highly-oriented crystals at the buried interface to the gate dielectric. High mobilities were attributed to a reduced number of grain boundaries as a consequence of a more uniform crystallite orientation. This interpretation is in good accordance with the outcome of X-ray and mobility experiments undertaken by Karl et al. on layers made from small molecules.[24]

On the contrary, Zen et al. considered that such layers consist of ordered domains with highly-planarized chains and disordered areas with coiled chains. The transport through the disordered areas was proposed to determine the carrier mobility on a macroscopic scale.[15] Zen et al. later showed that the nanorods seen in the AFM images of low molecular weight P3HTare actually embedded in an amorphous phase.[16] Also, a strong dependence of the melting temperature and melting enthalpy on chain length was shown. It was proposed that the amorphous areas consist mainly of very short chains (which are not able to crystallize) and that the macroscopic mobility is largely determined by the degree of crystallinity of the samples and not by the perfection of chain packing within the ordered domains. Further, detailed structural investigations revealed that the perfection of alignment of the crystalline domains in low molecular weight samples improves largely with decreasing layer thickness.[20] However, despite the very uniform orientation of the crystallites in ultra-thin layers, the field effect mobility remained low for all thicknesses. This was attributed to the presence of amorphous regions between highly crystalline domains.

Chang et al. investigated the morphology and transistor properties of P3HT fractions with high molecular weights ($M_w = 15\,000$ to $270\,000$ g mol^{-1}).[22] They found that the morphological nanostructure is largely determined by the speed of film formation, which may be varied by spin coating, drop-casting, or solvent parameters. Variations may give rise to extended nanoribbons, uniformly oriented nanoribbons (upon slow solvent evaporation), or comparatively amorphous structures with a bi-modal orientation of conjugated domains (upon fast solvent evaporation, e.g., by spin-coating from chloroform). For such fast-cast layers, the field-effect mobility was limited to relatively low values, which was explained by the presence of disordered regions.

High-resolution transmission electron microscopy (HR-TEM) on P3HT samples grown by directional epitaxial solidification clearly revealed the presence of disordered regions (denoted as amorphous interlamellar zones) between the rod-like nanocrystals.[5,19] It was shown that these effectively isolate the individual crystalline lamellae in samples of low molecular weight P3HT ($M_w = 7\,300$ g mol^{-1}). Interestingly, these studies revealed the presence of tie-crystallites for a molecular weight higher than 18 000 g mol^{-1}, constituting conjugated bridges between the ordered domains. It is, however, also worth mentioning that the sample preparation by Brinkmann et al. differs significantly from the spin-coating process commonly applied for OFET device preparation and that the conclusions drawn from those studies may not be valid for spin-coated samples.

A common result of the studies described above was that decreasing the molecular weight only has a small effect on the chain packing in the crystalline domains, despite a small decrease of the distance between the main chain (thiophene) layers and a concomitant increase in the π–π stacking distance. All studies agree in the interpretation that the crystallites in low molecular weight samples consist of fully extended chains, meaning that the width of these crystals is determined by the contour length.[16,17,19] It has also been proposed that the chains in high molecular weight samples fold back to form nanoribbons.[16,19,22,25] Besides these differences, the electronic properties of chain segments embedded in the crystalline domains should depend only weakly on molecular weight. In fact, a recent analysis of the optical absorption of P3HT in solution and the solid state revealed that the molecular weight has very little effect on the transition energies.[26,27] The significant increase of the 0–0 band at ~2.05 eV (or 600 nm) in absorption with higher molecular weight could be consistently explained by applying a model developed by Spano.[28,29] Hereby, the conjugated chains are assumed to form H-aggregates. In the limit of weak exciton coupling, the relative intensities of the individual transitions of the vibronic progression are mainly determined by the exciton bandwidth, which itself depends on the length of the correlated conjugated segments in the crystalline domains.[30] It was predicted that this length has rather little effect on the transfer integral, implying the rate of intermolecular hopping of carriers in crystalline domains shall be rather independent of the actual length of planarized chain segments.

In this paper, we present results on the local (nanoscopic) and macroscopic charge transport in layers of P3HT with different molecular weight. The local transport was probed as function of temperature by the measurement of the pulse-radiolysis time-resolved microwave conductivity (PR-TRMC), while the macroscopic transport properties were investigated in the common bottom-gate, top-contact organic field-effect transistor (OFET) geometry. We link these results with information on the length of planarized chain segments as obtained from a detailed analysis of the temperature-dependent UV/Vis absorption spectra. These data provide strong evidence that the mobility in samples from low and medium molecular weight P3HT is controlled by the probability of carriers to cross the disordered regions between nanocrystals.

2. Results and Discussion

The chemical structure of the investigated compound is drawn in Scheme 1. We investigated in detail two molecular weight fractions of regioregular P3HT (denoted by medium-MW and high-MW), the hexyl side chains of which have been deuterated (P3dHT) for potential use in neutron scattering. A former investigation on the molecular weight dependence of field-effect mobility and morphology of P3dHT and P3HT thin films did not reveal any difference in the physical properties of the deuterated fractions as compared to non-deuterated P3HT fractions.[15,16] Additionally, we report OFET and PR-TRMC mobility data of deuterated and

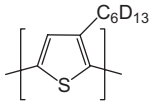

Scheme 1. Chemical structure of P3dHT.

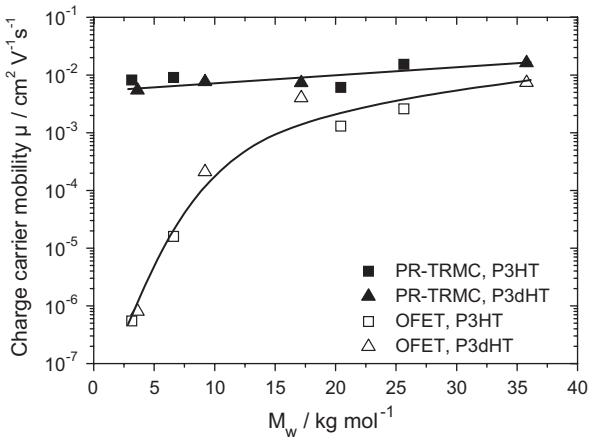

Figure 1. Molecular weight dependence of OFET and PR-TRMC charge carrier mobility of P3dHT and P3HT fractions at room temperature. The lines are guides to the eyes.

non-deuterated P3HT fractions of rather different molecular weight using the same polymer batches as in refs. [15,16].

2.1. Local (Nanoscopic) versus Macroscopic Transport

Figure 1 summarizes the local and macroscopic mobilities measured for deuterated and non-deuterated P3HT for various molecular weights at room temperature. PR-TRMC mobilities have been calculated from the after-pulse microwave conductivities, while the macroscopic OFET mobilities have been taken from the saturation regime of the output characteristics. As published earlier, the OFET mobility exhibits a pronounced increase with molecular weight. Contrary to this, the PR-TRMC values increase only slightly (by a factor of ~2) with chain length. Noticeably, the macroscopic mobility in high molecular weight P3HT differs only slightly from the value measured by PR-TRMC, while there is a huge difference when considering low molecular weights.

In PR-TRMC experiments the charge transport is probed on a local scale and charges moving back and forth inside a single grain of the material contribute mainly to the microwave conductivity signal. Therefore, PR-TRMC mobilities are generally expected to be higher than OFET mobilities, since in the former the mobility is not limited by the charge transport across grain boundaries or by charge carrier trapping on longer time scales. It should be noted that the PR-TRMC mobilities are the minimum values, assuming that all the charge that is initially generated survives until after the pulse. Since charges may decay by recombination and trapping already during the irradiation pulse, the actual microwave mobility is expected to be significantly higher. Due to this complication, it is difficult to compare absolute values for the microwave mobility with data obtained from OFET measurements.

2.1.1. Temperature-Dependent PR-TRMC Studies

In order to identify the processes leading to the difference between local and macroscopic transport in our P3HT samples, the temperature dependence of mobility has been studied in detail for two different molecular weights (Table 1). Also, measurements have been performed on a low-MW P3dHT fraction and the results

Table 1. Molecular parameters of the investigated molecular weight fractions of P3dHT (determined from GPC against polystyrene standards), including weight-average molecular weight (M_w), number-average molecular weight (M_n), and polydispersity index (PDI).

P3dHT fraction	M_w [g mol^{-1}]	M_n [g mol^{-1}]	PDI	Denotation
Hexane fraction	9 200	7 200	1.3	medium-MW fraction
Chloroform fraction	35 800	27 000	1.3	high-MW fraction

are presented in the Supporting Information. We find that low-MW P3dHT essentially behaves like the medium-MW fraction, however, transport and optical properties of the former are more severely affected at lower temperatures due to its lower melting point. During the PR-TRMC experiment the samples were heated step-wise from −75 to 120 °C and the transient microwave conductivity was recorded.

Figure 2a and b show PR-TRMC transients for the medium- and high-MW P3dHT fraction, respectively, at three different temperatures. Since the signal has been normalized to the dose, the absolute height of the signal is a direct measure of the change in conductivity induced per unit charge. For both samples the end-of-pulse conductivity increases with temperature, indicative of temperature-activated transport. Figure 3 summarizes the temperature dependence of the mobility extracted from these data. While these values are slightly lower for the medium-MW fraction, the temperature dependence above room temperature

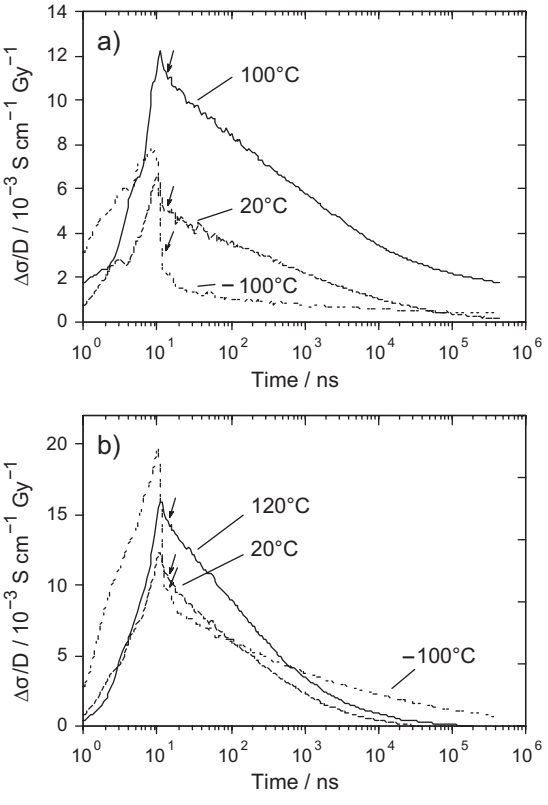

Figure 2. Microwave conductivity transients of the P3dHT medium-MW (a) and high-MW (b) fraction at different temperatures. End-of-pulse conductivities are marked by arrows.

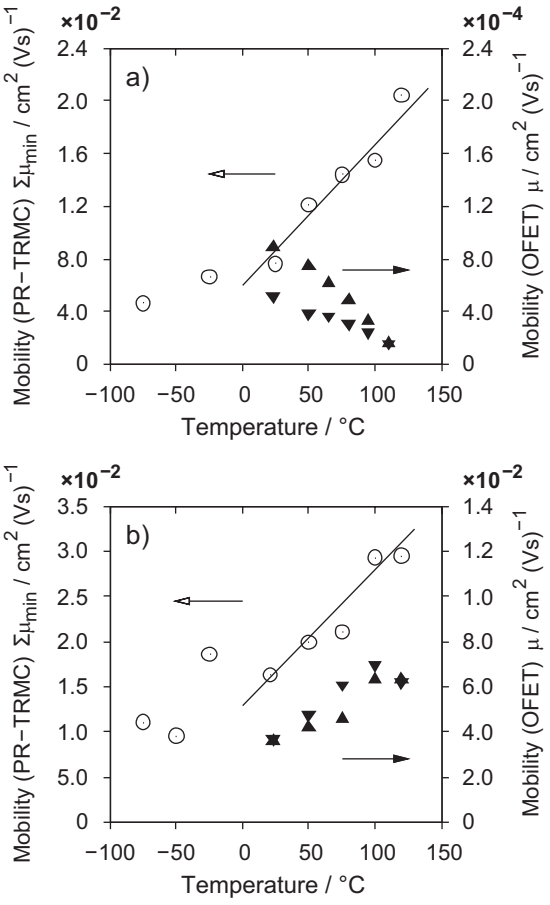

Figure 3. Temperature-dependent charge carrier mobilities of the P3dHT medium-MW (a) and high-MW (b) fraction from PR-TRMC (open symbols, during heating) and OFET experiments (filled symbols, upright and downward triangles during heating and subsequent cooling, respectively). The lines are guides to the eyes.

follows a rather similar trend for both samples. An increase of the microwave mobility with temperature has been often observed for organic conjugated materials and has been attributed to temperature-activated hopping over barriers or detrapping from shallow traps.[31–34] We also observed a rather high microwave mobility in our PR-TRMC studies on a low-MW P3dHT fraction (see Supporting Information). Here, the mobility increases continuously upon heating up to the melting temperature. At even higher temperatures, the mobility drops again, which we assign to the melting of the crystallites.

Regarding the transients shown in Figure 2, the decay characteristics are quite similar for both fractions, discarding the data measured at the lowest temperature of −100 °C. In a detailed study on high molecular weight P3HT samples, this decay has been attributed to carrier trapping rather than recombination with opposite free charges.[31] A good fit to the experimental after-pulse transients was obtained by assuming first-order decay (see Supporting Information), meaning that the number of traps is constant over time and significantly larger than the number of mobile charges generated in the PR-TRMC experiment.

From these fits, the mean decay times have been computed. For both fractions we find the decay times to increase with temperature (see Table S1 of the Supporting Information). This observation is consistent with the assumption drawn from earlier temperature-dependent microwave mobility data that the transport is determined by temperature-activated transport in a density-of-states distribution, where the charges are detrapped from shallow traps at higher temperature that would otherwise remain immobilized at low temperatures.[31,35] On the other hand, the rather rapid initial decay of the microwave conductivity signal at low temperatures (Fig. 2) is assigned to the immobilization of charges by shallow traps, leading to a fast decay of the number of free charges that initially contribute to the microwave conductivity signal.

Interestingly, the decay of the conductivity signal for the medium-MW fraction at room temperature and above is rather slow (slower than for the high-MW fraction, compare Fig. 2a and b), meaning that the carriers created in this sample are less susceptible to immobilization. Taking into account the rather similar intra-grain mobilities of charges in high- and medium-MW P3dHT (and low-MW P3dHT as well; see Supporting Information), this implies that chain ends (the density of which is higher in the short-chain medium-MW fraction) or grain boundaries do not affect the carrier transport on a local scale.

2.1.2. Temperature-Dependent OFET Mobilities

Charge carrier mobilities were extracted from the OFET characteristics at different temperatures in a cycle of heating from 25 to 120 °C (110 °C for the medium-MW fraction) and subsequent cooling back to room temperature and these values are also shown in Figure 3. The temperature dependence is clearly different for both fractions, where a decrease in the mobility of the medium-MW P3dHT sample is opposed to a strong increase in the mobility of the long-chain high-MW fraction. Similar like for the medium-MW fraction, OFETs made from low-MW P3dHT show a decrease of mobility at 50 °C as compared to room temperature (see Supporting Information).

Note that we have recently reported a significant drop of the OFET mobility above ~100 °C for a different P3HT sample with intermediate molecular weight.[23] Extensive X-ray studies on these layers suggested that the impairment of transport properties at higher temperatures cannot be explained by thermally induced morphological changes within the well-ordered crystalline domains, but that this effect must be related to inter-grain transport properties (i.e., the transport through disordered domains). Indeed, the π–π stacking of the aggregated P3HT chains has been shown to stay intact even up to temperatures close to melting (~220 °C). Moreover, we found the in-plane π–π stacking distance to be slightly reduced above 50 °C as compared to room temperature—the expected benefit of this reduction with regard to intra-grain transport was, however, not reflected in the temperature-resolved mobility measurements.

The analysis of the OFET mobility data of the high-MW fraction yields an activation energy of ~60 meV, which is quite comparable to 54 meV as reported by Kline et al. for another high molecular weight P3HT fraction ($M_n = 35\,000$ g mol^{-1}) below room temperature.[11] Interestingly, our experiments yield a rather

similar temperature dependence of the microwave mobility and the OFET mobility for our high-MW P3dHT. Although absolute mobility values are difficult to compare, as pointed out above, similar activation energies for transport on the local and macroscopic scale suggest that charges can move rather freely between crystalline domains, without the need to overcome significant energy barriers.

On the other hand, the data summarized above for medium-MW P3dHT provide convincing proof for the conclusions from structural studies, that the transport of charges over larger distances is actually not determined by the local motion within the individual grains, but by the morphological heterogeneity of the sample, namely the presence of disordered areas in-between crystallites.

2.2. In situ Thermal Dependence of UV/Vis Absorption

A. Zen et al. have shown that the absorption of solid layers of short chain P3HT exhibits a significant blue shift when heating the sample above room temperature.[16] Pronounced spectral changes of absorption as a function of temperature (thermochroism) are generally known for polythiophenes and are explained in terms of a thermally-induced conformational variation of the absorbing molecules.[36–43] It is believed that heating causes the conjugated molecular backbones to deplanarize by enhanced twisting between adjacent thiophene units, resulting in shorter conjugation lengths and wider conjugation length distribution. This very qualitative explanation was further supported by temperature-dependent X-ray investigations, showing that the packing of molecular chains is indeed affected already below melting temperature.[40,44]

Figure 4a shows absorption spectra measured at different temperatures for a layer of medium-MW P3dHT. Upon increasing the temperature, the absorption maximum blue-shifts continuously and looses absorption strength. In particular, the strength of the 2.05 eV (600 nm) transition reduces rapidly with temperature, pointing to significant changes of the nanomorphology. After cooling, the initial absorption is almost recovered, including the reoccurrence of the vibronic structure. The same behavior is found for low-MW P3dHT (see Supporting Information); however, the vibronic structure is far less distinctive than for medium-MW P3dHT due to the lower crystallinity of low-MW P3dHT.[16] Note that all spectra have been recorded at temperatures below the melting transition, which occurs above 150 °C, for medium-MW P3dHT (see the differential scanning calorimetry (DSC) scan inserted in Fig. 4a). For comparison, the absorption of the high-MW P3dHT fraction is shown in Figure 4b, where the thermally induced blue shift is far less pronounced and completely reversible. The DSC scan inset in Figure 4b shows that the melting transition of high-MW P3dHT occurs above 220 °C, which is much higher than the maximum temperature applied in our optical and electrical studies.

J. Clark et al.[45,46] published a sound analysis of the optical absorption data of P3HT layers with respect to the film nanostructure, using a model by Spano.[28,29] In general, the absorption of P3HT in the solid state consists of a low energy vibronic progression attributed to the absorption by planarized chains contained in aggregates, and a broad high-energy part caused by twisted chains in disordered areas. This assignment is

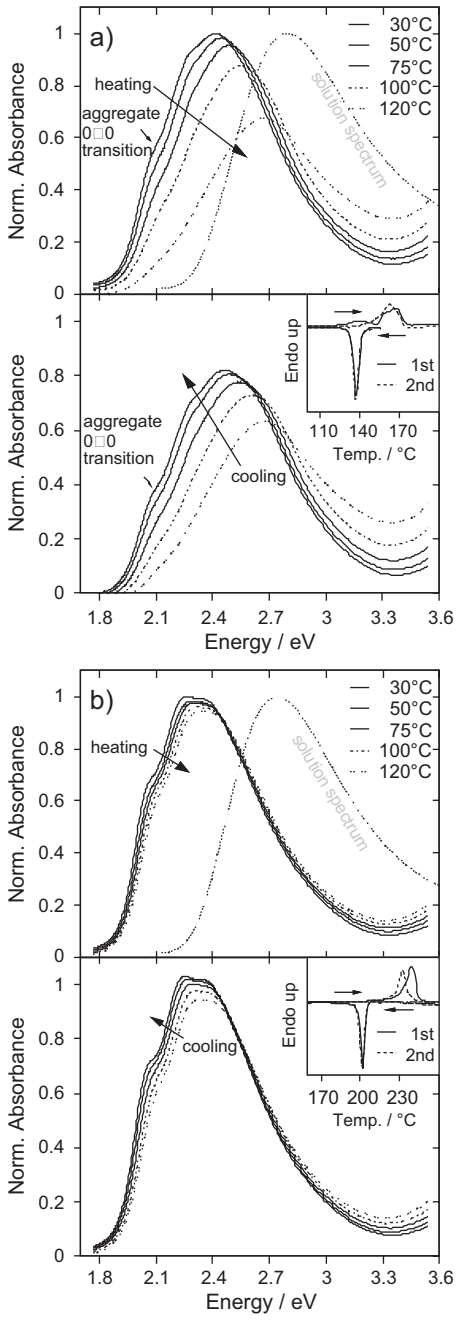

Figure 4. Temperature-dependent UV/Vis absorption of medium-MW (a) and high-MW (b) P3dHT layers during a cycle of heating (upper graphs) and subsequent cooling (lower graphs). The spectra have been normalized to the maximum absorption at 30 °C. Spectra in solution are plotted for comparison. The insets show DSC thermograms of respective solution-crystallized P3dHT samples.

supported by the rather blue-shifted and featureless absorption of P3HT in dilute solution.

As pointed out in the Introduction, Spano modeled the optical properties of P3HT films by assuming the formation of H-aggregates of parallel-aligned cofacially-packed conjugated chains.[28,29] In the case of weak excitonic coupling, the splitting of the electronic levels due to Coulombic interactions is

considerably smaller than the vibrational energy.[28,29,47] As a consequence, interchain coupling leads to a formation of vibronic bands, with their width basically being determined by the exciton bandwidth W. For symmetry reasons, only transitions from the ground state to the highest energy states of these individual bands are optically allowed. In this limit, the aggregate absorption of P3HT can be modeled according to

$$A \propto \sum_{m=0} \left(\frac{S^m}{m!}\right) \cdot \left(1 - \frac{We^{-S}}{2E_p} \sum_{n \neq m} \frac{S^n}{n!(n-m)}\right)^2 \cdot \exp\left(\frac{\left(E - E_0 - mE_p - \frac{1}{2}WS^m e^{-S}\right)^2}{2\sigma^2}\right), \quad (1)$$

where E_0 is the 0–0 transition energy of the aggregated species, E_p is the frequency of the vibronic transition, σ is the width of the line shape that is assumed to be Gaussian, S is the electron–phonon coupling strength (Huang-Rhys factor) and m counts the vibrational excitation. Hereby, the squared pre-factor in brackets is a modification of the Franck–Condon factor including interband mixing. The transition energies are corrected for the blue shift due to the energy splitting, considering only excitations to the top of the exciton bands to be optically allowed. Equation (1) neglects, however, that transitions to lower states within the vibronic bands become weakly allowed if disorder is introduced into the aggregates. It, additionally, assumes that the linewidth σ is the same for all transitions. Evidently, the exciton bandwidth W affects both the position and the relative strength of the individual vibronic transitions. As pointed out in the original paper by Spano,[29] increasing W causes a considerable reduction of the relative 0–0 transition strength. As shown later by Beljonne et al. and Gierschner et al., W is related to the length of the cofacially arranged chain segments L in the crystallites (Fig. 5), which shall be equivalent to the width of the nanoribbons seen in the structural studies described above.[30,48]

We have used Equation (1) to model the aggregate part of our temperature dependent P3dHT spectra. Hereby, we considered all terms up to the 0–6 transition. In the fitting procedure, E_0, σ, W, and a global factor were varied as free parameters, while S and E_p were fixed to 1.0 and 0.179 eV, respectively, as reported in the literature.[22,28,29,45,46,49,50] In P3HT, the main vibrational mode coupled to the UV/Vis electronic transition is known to be the C=C symmetric stretch at 0.179 eV.[49,51] The main difficulty to fit model Equation (1) to the absorption spectra was to identify the contribution stemming from aggregated chains. Experimental and simulated absorption spectra reported by Clark et al. suggested that contributions of non-aggregated molecules should be insignificant at energies below ~2.3 eV.[45] In order to test the consistency of the best-fit parameters, we varied the energy range used to fit the spectra to Equation (1) (see Supporting Information). The values of E_0, σ, and W were found to vary only slightly (max. ±0.5%, ±2%, ±4%, for E_0, σ, W, respectively) within lower and upper bounds of 1.92–2.05 and 2.20–2.35 eV, respectively. Thus, we considered the spectral range from 2.00 to 2.30 eV for the following analysis.

Figure 6 shows exemplary fits of absorption spectra of medium-MW P3dHT recorded at 50 and 120 °C. Further examples for fits to the spectra of the medium- and high-MW fractions are included in the Supporting Information. The black line of the model spectra reproduces very well both 0–0 and 0–1 intermolecular transition features. The difference between the experimental and calculated spectra (lines and filled circles) mostly represents the amorphous phase in the sample, although it is not fully identical to the absorption of P3HT chains in dilute solution. Possibly, the different environment of the chains in the disordered solid state and in solution is mainly responsible for this shift. In addition, the residual is weakly structured, indicating that the fit to Equation (1) does not fully explain the aggregate absorption spectrum over the whole wavelength range. As pointed out above, the applied model does not account for transitions to lower energy states in the vibrational bands, which become weakly allowed due to disorder. Additionally, our choice of a Gaussian line shape might be too simplistic for aggregate absorption.

The best-fit parameters of the aforementioned procedure are summarized in Figure 7. Values for the transition energy E_0 and for the line width σ are relatively similar for both medium- and high-MW samples. Additionally, both samples show the same weak dependence of temperature on E_0. This suggests that the local electronic properties of the chains in the ordered domains are only weakly affected by the molecular weight, in accordance with the results from the PR-TRMC studies described above. Upon heating from 30 to 120 °C, the intermolecular 0–0 transition energy increases by maximal 40 meV, corresponding to a blue shift of only 10 nm for the aggregates of both fractions. We assign this to thermally-induced local torsions of the conjugated backbones within the aggregates. This shift appears to be

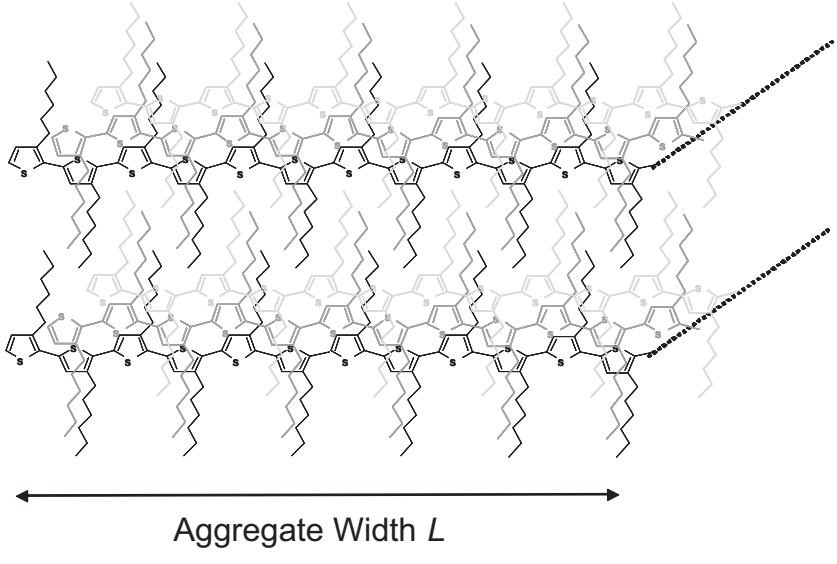

Figure 5. Schematic sketch of the molecular arrangement in a P3HT aggregate (medium-MW fraction, i.e., no chain folding present). The crystallite's long axis is indicated with dotted lines (as virtual third dimension).

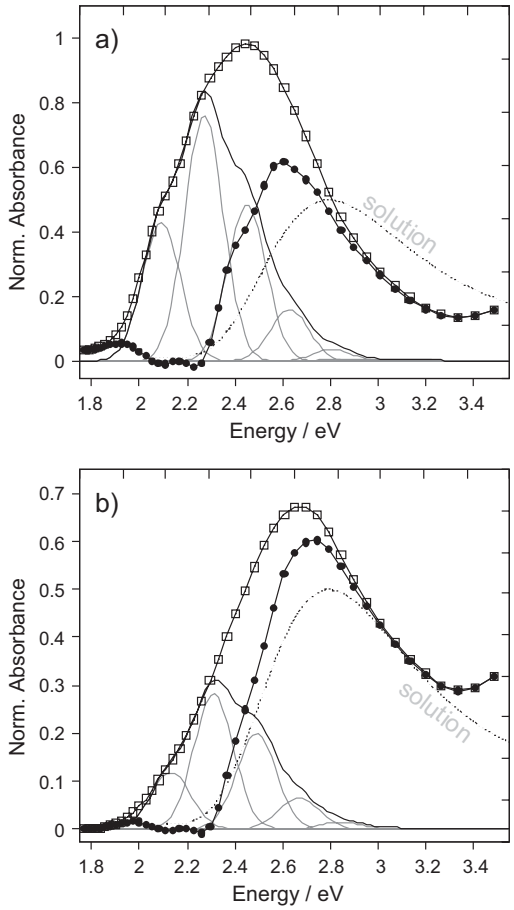

Figure 6. Absorption spectra of medium-MW P3dHT at a) 50 and b) 120 °C (lines and open squares). The spectra have been normalized to the maximum absorption of the 30 °C spectra (Fig. 4). The best-fits according to Equation (1) to the region of aggregate absorption (2.0–2.3 eV) are shown as bold lines, as well as the individual electronic-vibrational transitions (thin grey lines). The differences of the experimental and aggregate model spectra are displayed as lines and filled circles. The spectra of P3dHT in chloroform solution are plotted for comparison (dotted lines, normalized to 0.5).

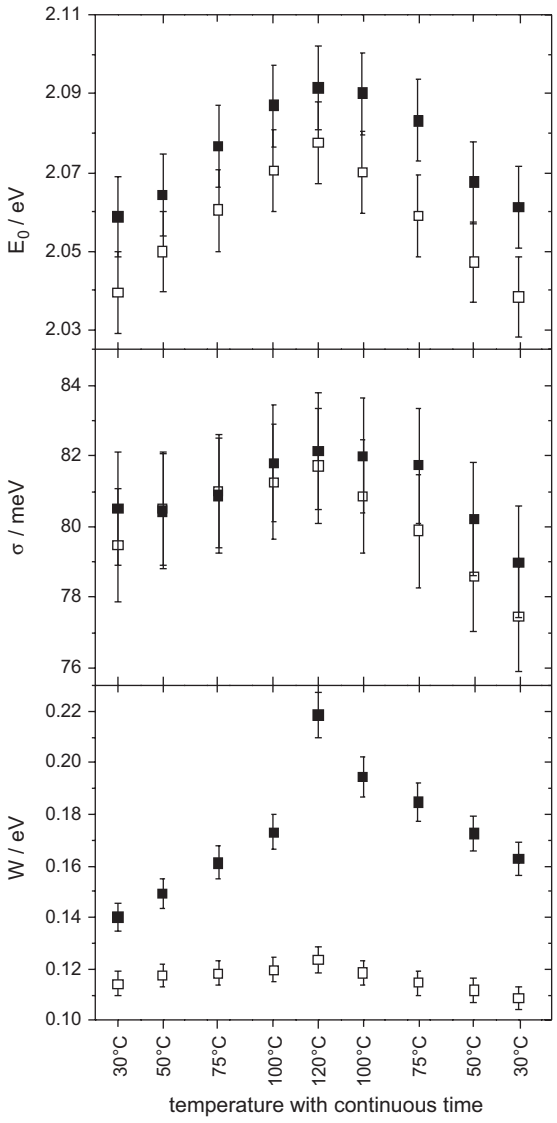

Figure 7. Parameters of the best-fits of Equation (1) to the experimental spectra of medium-MW (solid symbols) and high-MW P3dHT (open symbols) in the region of aggregate absorption (2.0–2.3 eV). E_0, σ and W are the 0–0 intermolecular transition energy, the width of the Gaussian line shape, and the exciton bandwidth, respectively.

insignificant regarding the large spectral changes occurring upon heating for the medium-MW sample in Figure 4a and even when considering the apparent blue shift of the absorption maximum for the high-MW fraction in Figure 4b.

The evaluation of the spectra shows that the thermal dependence of the absorption includes, in addition to the minor blue shift, an overall decrease of the aggregate absorption (Fig. 6 and Supporting Information) and also a significant redistribution of the oscillator strength within the aggregate absorption. The latter can be attributed to a change of the exciton band width in the aggregates of cofacially arranged chains with temperature. In fact, the value of W extracted from the fits is markedly higher for the medium-MW batch and it increases strongly with temperature (while for high-MW P3dHT the free exciton bandwidth remains almost constant over the whole temperature region, Fig. 7). For a large number of chains in an aggregate, the free exciton bandwidth W is twice the exciton coupling strength V_{AB}. Gierschner et al.[30] have performed theoretical calculations on aggregates of thiophene chains with N repeat units (determining the correlation length L) for different values of the intermolecular distance and the number of interacting aggregated chains. According to these calculations, the observed increase in W when heating the medium-MW layer can be caused by *a)* a decrease of the intermolecular π–π stacking distance, *b)* a larger number of molecules constituting the aggregate, and *c)* a smaller correlation length.

In recent X-ray studies we observed a slight decrease of the relevant π–π stacking distance by 3% when the layer was heated from room temperature to its melting regime (starting from ~220 °C).[23] Surprisingly, this decrease occurred abruptly at 50 °C and the intermolecular distance remained constant at higher temperatures. In contrast, the increase of W with temperature

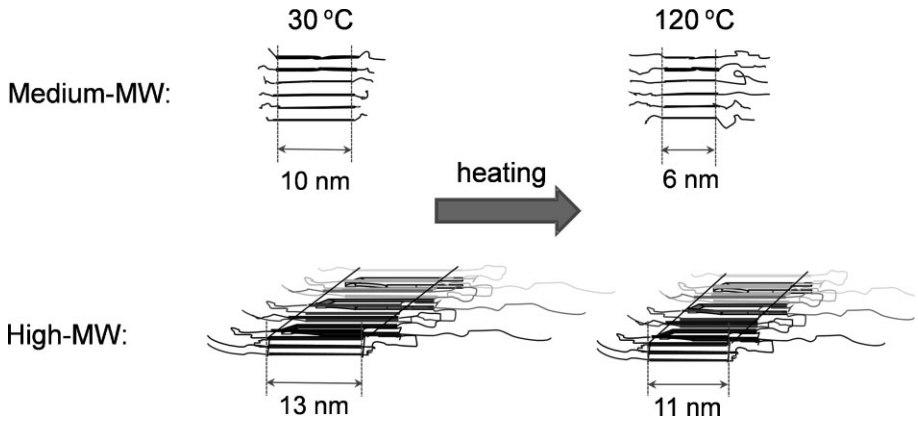

Figure 8. Visualization of the effect of heating of the P3dHT aggregates below the melting temperature.

is continuous, ruling out that the temperature-induced change in stacking distance is the main cause of the continuous and reversible increase of *W*.

An increase of the number of aggregated molecules, i.e., a growth of crystal size with increasing temperature, which is reversible upon cooling, does not seem plausible. Crystal growth during annealing is a known effect and might be the origin of the offset (~20 meV) between the free exciton bandwidths before and after annealing. The shrinkage of the aggregate size upon cooling is, however, highly unlikely.

As a result, we attribute the increase of the free exciton bandwidth in medium-MW P3dHT to the shortening of the interacting conjugated segments upon heating. The process is visualized in Figure 8. Using the simulation data from Gierschner et al. (Fig. 9), an exciton bandwidth of 140 meV, as found for medium-MW P3dHT at room temperature, is equivalent to ~25 interacting repeat units (or an interacting chain length of ~10 nm). This is nearly equivalent to the contour length of the medium-MW chains (27 repeat units on average after molecular weight correction according to Liu et al.[52]), which means that the chains are fully elongated within the aggregates. This result is fully consistent with the findings from structural studies as discussed above. Upon heating to 120 °C, the interacting chain length shortens towards 16 repeat units (equivalent to ~6 nm). This process occurs well below the actual melting temperature of the sample, implying that the medium-MW P3dHT aggregates undergo a "pre-melting," probably starting from its edges.

In high-MW P3dHT the temperature dependence of the exciton bandwidth is much less pronounced: *W* increases nearly reversibly from 114 to 123 meV upon heating from room temperature to 120 °C. This corresponds to a change from 31 to 28 interacting repeat units (or ~12.5 to 11 nm), compared to a contour length of ~26.5 nm). One possible reason for this weak effect of temperature on the interaction length may be the higher melting temperature of the high-MW P3dHT fraction. Alternatively, the number of chains folding back into the same aggregates might become larger with increasing chain length, as suggested by Brinkmann[19] and such backfolds might impede the pre-melting from the edges of the crystallites.

It is worth noting that the thermochroism in our medium-MW sample is characterized by a *continuous* blue shift and that it does not exhibit an isosbestic point. A similar situation was encountered by Holdcroft and co-workers when studying the thermochroism of high-MW regioregular P3HT at higher temperatures.[40] They suggested that this continuous blue shift is caused by the transition between three (rather than two) phases with distinctive absorption properties, namely a crystalline, a quasi-ordered, and a disordered phase. This interpretation was, however, based on the presumption that the absorption of the crystalline phase is independent of temperature. Our analysis of thermochroism in medium-MW P3HT shows conclusive evidence for a significant redistribution of oscillator strength between the individual vibronic transitions upon heating. Thereby, increasing the temperature causes transitions to higher vibronic states to become more intense. As a result, the overall envelope of the crystalline absorption appears to blue-shift with temperature, though the individual transition energies remain almost unaffected.

3. Conclusions

Our investigation of the intragrain charge transport in solid P3HT by pulse-radiolysis microwave conductivity reveals that the local mobility depends only weakly on molecular weight, despite the large effect of chain length on the OFET performance. Local transport is temperature-activated for the low-, medium- and high-MW P3dHT fractions well below the melting temperature,

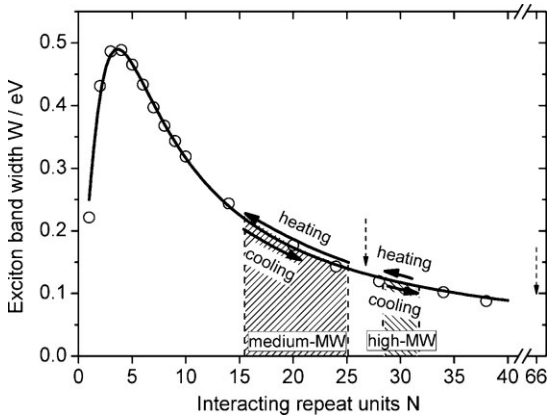

Figure 9. Dependence of the exciton bandwidth on the interacting chain length of aggregated P3HT molecules in terms of planarized thiophene repeat units. Circles show the results of simulations by Gierschner et al. (ref. [30], Fig. 3,) on the exciton coupling energy as function of the number of interacting thiophene rings, taking into account screening effects. The solid curve is a guide to the eye. Bold arrows display the evolution of the interacting chain length upon heating and cooling, as obtained from the analysis of the absorption spectra in Figure 4. Dashed arrows mark the average contour chain length of medium- and high-MW P3dHT as calculated from the number averages in Table 1 and the molecular weight correction according to Liu et al. [52]. Portions adapted with permission from Reference [30]. Copyright 2009, American Institute of Physics.

which can be attributed to hopping in a density-of-states distribution.

In contrast to the local transport properties, we found that the macroscopic mobility of medium-MW P3dHT layers is two orders of magnitude lower than the local mobility and it decreases with increasing temperature. The striking differences of charge transport at both length scales are related to the layer nanomorphology. From the comparison of local and macroscopic mobilities, we conclude that macroscopic transport is not actually determined by the local motion of charges within ordered grains, but by the transport through disordered material surrounding these grains.

The quantitative analysis of temperature-dependent UV/Vis absorption spectra suggests that the aggregates in medium-MW P3dHT undergo a "pre-melting" significantly below the actual melting temperature. As a result, the interacting chain length (i.e., the number of interacting repeat units) of the molecules that constitute an aggregate becomes smaller, i.e., the aggregate width decreases. The concomitant increase in width of the interlamellar zones, as well as the likely increase of disorder in these amorphous regions (as evidenced by the blue-shift of the absorption of the disordered phase) is presumably the main reason for the drop in the macroscopic mobility of short chain P3dHT upon heating. In contrast, long chains may interconnect the crystalline domains in high-MW P3dHT, thus by-passing the disordered interlamellar regions, and rendering the macroscopic charge transport in this material less susceptible to changes of the sample heterogeneity.

4. Experimental

For the investigations, P3dHT was prepared by the Grignard metathesis procedure according to McCullough and co-workers [53]. The deuteration of side chains was chosen in order to perform neutron scattering experiments, which are the subject of further investigations. The raw polymer was fractionated by applying the solvent extraction method [54]. Subsequent extraction steps, with solvents of increasing solubility for P3dHT, yielded polymer fractions with polydispersity indices between 1.3 and 1.4. The average molecular weights were determined by using gel permeation chromatography (GPC) with THF as the solvent (calibration with narrowly distributed polystyrene standards). Powders of the P3dHT fractions were precipitated from solvents into non-solvents, where such powders are often highly crystalline.

Optical absorption spectra were measured in situ with a Perkin-Elmer Lambda 19 UV/Vis spectrometer at various temperatures. Thin polymer films (~50–80 nm in thickness) were spin-coated from chloroform solutions (typically 10 g L^{-1}) on glass substrates that were covered by a transparent indium tin oxide (ITO) electrode on the backside. The sample temperature was controlled by resistive heating of the ITO, where the actual temperature at the polymer surface was measured using a PT100 temperature sensor glued to the front side of the substrate. For technical reasons, the maximum temperature was 120 °C.

PR-TRMC was performed in order to investigate the local charge transport properties. Details about the instrumentation and sample preparation can be found in refs. [31,55,56]. The sample is contained in a microwave cell with rectangular dimensions. Pulsed irradiation with high-energy (3 MeV) electrons leads initially to a low (micro-molar) concentration of positive and negative charge carriers uniformly distributed in the samples. After the incident pulse (1–50 ns duration), the conductivity of the sample is probed as a function of time by monitoring the attenuation of a reflected microwave (frequency range of 28–38 GHz and maximum electric field strength of 10 V m^{-1}). The fractional change in microwave power reflected by the cell is directly proportional to the change in conductivity ($\Delta\sigma$). The concentration of charges that is generated initially can be estimated using dosimetry measurements [57]. Using this estimation the charge carrier mobility can be calculated. Due to trapping or charge carrier recombination during the pulse, PR-TRMC results in a lower limit for the charge carrier mobility (μ_{min}). As both positive and negative charge carriers can contribute to the conductivity signal, μ_{min} represents the sum of hole and electron mobility, the latter is expected to be negligible in P3HT [31]. For a more detailed description of the PR-TRMC technique see refs. [31,56].

For the investigation of charge transport covering macroscopic distances we evaluated the electrical properties of OFETs. In the present OFET geometry, charge carriers—primarily holes in case of P3HT on top of SiO_2—have to move 100 μm from the source to the drain electrode through the polymer layer, parallel and close to the semiconductor-insulator surface. Assuming a domain size of 10 nm [16], holes have to cross 10 000 domains and domain boundaries for crossing the channel. Therefore, the field-effect mobility, as calculated from OFET characteristics, is a macroscopic effective value that results from all local mobilities within the different domains and from potential transport barriers at the domain boundaries.

OFETs were prepared in bottom-gate, top-source/drain geometry. Homogeneous polymer layers with a thickness in the range of 50–80 nm were formed by spin-coating from chloroform solution onto n-doped silicon substrates that are covered with a ~300 nm thick insulating SiO_2 layer. Prior to all processing, the SiO_2 surface was thoroughly cleaned with several common solvents and underwent an oxygen plasma treatment (5 min at a power of 200 W), followed by silanization using hexamethyldisilazane (HMDS) for 26 h at 60 °C. Finally, 100 nm thick evaporated interdigitating gold electrodes served as source and drain contacts. Device characteristics at specific temperatures were recorded using an Agilent 4155C semiconductor parameter analyzer. The temperature was controlled using a Digit Concept DCT 600 thermal controller and heating chuck. Preparation and measurements were performed in an inert nitrogen atmosphere. Charge carrier mobilities were calculated from the saturation region of the output characteristics (drain current, I_{DS} vs. source-drain voltage, V_{DS}) according to

$$I_{DS,sat} = \frac{WC_i}{2L}\mu_{sat}(V_{DS} - V_0)^2, \quad (2)$$

where $W = 14.85$ cm and $L = 100$ μm are the channel width and length, respectively, $C_i = 11.9$ nF cm^{-2} is the capacitance per unit area and V_0 is the onset voltage.

Acknowledgements

We thank Dr. S. Janietz, Fraunhofer Institute for Applied Polymer Research, Potsdam, and Prof. Dr. U. Scherf, University of Wuppertal for providing the molecular weight fractions of P3dHT. We are grateful to Sarah Turner for her valuable help editing the manuscript. This work was financially supported by the Deutsche Forschungsgemeinschaft, Schwerpunktprogramm 1121. Supporting Information is available online from Wiley InterScience or from the author.

Received: December 1, 2009
Revised: March 30, 2010
Published online: June 14, 2010

[1] *Organic Electronics*, (Ed: K. Hecker), VDMA Verlag GmbH, Germany **2007**.
[2] Z. Bao, *Adv. Mater.* **2000**, *12*, 227.
[3] A. Dodabalapur, *Mater. Today* **2006**, *9*, 24.
[4] S. P. Speakman, G. G. Rozenberg, K. J. Clay, W. I. Milne, A. Ille, I. A. Gardner, E. Bresler, J. H. G. Steinke, *Org. Electron.* **2001**, *2*, 65.
[5] M. Brinkmann, P. Rannou, *Adv. Funct. Mater.* **2007**, *17*, 101.
[6] J. F. Chang, B. Q. Sun, D. W. Breiby, M. M. Nielsen, T. I. Solling, M. Giles, I. McCulloch, H. Sirringhaus, *Chem. Mater.* **2004**, *16*, 4772.

[7] D. M. DeLongchamp, B. M. Vogel, Y. Jung, M. C. Gurau, C. A. Richter, O. A. Kirillov, J. Obrzut, D. A. Fischer, S. Sambasivan, L. J. Richter, E. K. Lin, *Chem. Mater.* **2005**, *17*, 5610.
[8] H. Yang, T. J. Shin, L. Yang, K. Cho, C. Y. Ryu, Z. Bao, *Adv. Funct. Mater.* **2005**, *15*, 671.
[9] R. J. Kline, D. M. DeLongchamp, D. A. Fischer, E. K. Lin, L. J. Richter, M. L. Chabinyc, M. F. Toney, M. Heeney, I. McCulloch, *Macromolecules* **2007**, *40*, 7960.
[10] R. J. Kline, M. D. McGehee, E. N. Kadnikova, J. S. Liu, J. M. J. Frechet, *Adv. Mater.* **2003**, *15*, 1519.
[11] R. J. Kline, M. D. McGehee, E. N. Kadnikova, J. S. Liu, J. M. J. Frechet, M. F. Toney, *Macromolecules* **2005**, *38*, 3312.
[12] H. Sirringhaus, *Adv. Mater.* **2005**, *17*, 2411.
[13] H. Sirringhaus, P. J. Brown, R. H. Friend, M. M. Nielsen, K. Bechgaard, B. M. W. Langeveld-Voss, A. J. H. Spiering, R. A. J. Janssen, E. W. Meijer, P. Herwig, D. M. de Leeuw, *Nature* **1999**, *401*, 685.
[14] G. M. Wang, J. Swensen, D. Moses, A. J. Heeger, *J. Appl. Phys.* **2003**, *93*, 6137.
[15] A. Zen, J. Pflaum, S. Hirschmann, W. Zhuang, F. Jaiser, U. Asawapirom, J. P. Rabe, U. Scherf, D. Neher, *Adv. Funct. Mater.* **2004**, *14*, 757.
[16] A. Zen, M. Saphiannikova, D. Neher, J. Grenzer, S. Grigorian, U. Pietsch, U. Asawapirom, S. Janietz, U. Scherf, I. Lieberwirth, G. Wegner, *Macromolecules* **2006**, *39*, 2162.
[17] R. Zhang, B. Li, M. C. Iovu, M. Jeffries-El, G. Sauve, J. Cooper, S. J. Jia, S. Tristram-Nagle, D. M. Smilgies, D. N. Lambeth, R. D. McCullough, T. Kowalewski, *J. Am. Chem. Soc.* **2006**, *128*, 3480.
[18] J. M. Verilhac, R. Pokrop, G. LeBlevennec, I. Kulszewicz-Bajer, K. Buga, M. Zagorska, S. Sadki, A. Pron, *J. Phys. Chem. B* **2006**, *110*, 13305.
[19] M. Brinkmann, P. Rannou, *Macromolecules* **2009**, *42*, 1125.
[20] S. Joshi, S. Grigorian, U. Pietsch, P. Pingel, A. Zen, D. Neher, U. Scherf, *Macromolecules* **2008**, *41*, 6800.
[21] R. J. Kline, M. D. McGehee, M. F. Toney, *Nat. Mater.* **2006**, *5*, 222.
[22] J. F. Chang, J. Clark, N. Zhao, H. Sirringhaus, D. W. Breiby, J. W. Andreasen, M. M. Nielsen, M. Giles, M. Heeney, I. McCulloch, *Phys. Rev. B* **2006**, *74*, 115318.
[23] S. Joshi, P. Pingel, S. Grigorian, T. Panzner, U. Pietsch, D. Neher, M. Forster, U. Scherf, *Macromolecules* **2009**, *42*, 4651.
[24] N. Karl, in: *Organic Electronic Materials*, (Eds: R. Farchioni, G. Grosso), Springer, Berlin **2001**.
[25] S. Malik, A. K. Nandi, *J. Polym. Sci. Part. B: Polym. Phys.* **2002**, *40*, 2073.
[26] R. Kalbitz, diploma thesis, Universität Potsdam **2008**.
[27] R. Kalbitz, F. Jaiser, S. Nahar, M. Forster, S. Allard, U. Scherf, D. Neher, A. Köhler, unpublished.
[28] F. C. Spano, *Chem. Phys.* **2006**, *325*, 22.
[29] F. C. Spano, *J. Chem. Phys.* **2005**, *122*, 234701.
[30] J. Gierschner, Y. S. Huang, B. Van Averbeke, J. Cornil, R. H. Friend, D. Beljonne, *J. Chem. Phys.* **2009**, *130*, 044105.
[31] G. Dicker, M. P. de Haas, J. M. Warman, D. M. de Leeuw, L. D. A. Siebbeles, *J. Phys. Chem. B* **2004**, *108*, 17818.
[32] G. H. Gelinck, J. M. Warman, *J. Phys. Chem.* **1996**, *100*, 20035.
[33] P. Prins, F. C. Grozema, B. S. Nehls, T. Farrell, U. Scherf, L. D. A. Siebbeles, *Phys. Rev. B* **2006**, *74*, 113203.
[34] J. M. Warman, G. H. Gelinck, M. P. de Haas, *J. Phys. Condes. Matter* **2002**, *14*, 9935.
[35] G. Dicker, M. P. de Haas, D. M. de Leeuw, L. D. A. Siebbeles, *Chem. Phys. Lett.* **2005**, *402*, 370.
[36] S. Garreau, M. Leclerc, N. Errien, G. Louarn, *Macromolecules* **2003**, *36*, 692.
[37] O. Inganäs, G. Gustafsson, W. R. Salaneck, J. E. Osterholm, J. Laakso, *Synth. Met.* **1989**, *28*, C377.
[38] O. Inganäs, in: *Handbook of Organic Conductive Molecules and Polymers*, (Ed: H. S. Nalwa), John Wiley & Sons Ltd, New York **1997**, pp. 785–793.
[39] O. Inganäs, W. R. Salaneck, J. E. Osterholm, J. Laakso, *Synth. Met.* **1988**, *22*, 395.
[40] C. Yang, F. P. Orfino, S. Holdcroft, *Macromolecules* **1996**, *29*, 6510.
[41] K. Iwasaki, H. Fujimoto, S. Matsuzaki, *Synth. Met.* **1994**, *63*, 101.
[42] W. R. Salaneck, O. Inganäs, J. O. Nilsson, J. E. Osterholm, B. Themans, J. L. Brédas, *Synth. Met.* **1989**, *28*, C451.
[43] W. R. Salaneck, O. Inganas, B. Themans, J. O. Nilsson, B. Sjogren, J. E. Osterholm, J. L. Brédas, S. Svensson, *J. Chem. Phys.* **1988**, *89*, 4613.
[44] S. Hugger, R. Thomann, T. Heinzel, T. Thurn-Albrecht, *Colloid Polym. Sci.* **2004**, *282*, 932.
[45] J. Clark, C. Silva, R. H. Friend, F. C. Spano, *Phys. Rev. Lett.* **2007**, *98*, 206406.
[46] J. Clark, J. F. Chang, F. C. Spano, R. H. Friend, C. Silva, *Appl. Phys. Lett.* **2009**, *94*, 163306.
[47] *Electronic Processes in Organic Crystals and Polymers*, (Eds: M. Pope, C. E. Swenberg), Oxford University Press, New York **1999**.
[48] D. Beljonne, J. Cornil, R. Silbey, P. Millie, J. L. Brédas, *J. Chem. Phys.* **2000**, *112*, 4749.
[49] P. J. Brown, D. S. Thomas, A. Köhler, J. S. Wilson, J. S. Kim, C. M. Ramsdale, H. Sirringhaus, R. H. Friend, *Phys. Rev. B* **2003**, *67*, 064203.
[50] F. C. Spano, J. Clark, C. Silva, R. H. Friend, *J. Chem. Phys.* **2009**, *130*, 074904.
[51] A. Ruseckas, E. B. Namdas, T. Ganguly, M. Theander, M. Svensson, M. R. Andersson, O. Inganäs, V. Sundstrom, *J. Phys. Chem. B* **2001**, *105*, 7624.
[52] J. S. Liu, R. S. Loewe, R. D. McCullough, *Macromolecules* **1999**, *32*, 5777.
[53] R. S. Loewe, S. M. Khersonsky, R. D. McCullough, *Adv. Mater.* **1999**, *11*, 250.
[54] M. Trznadel, A. Pron, M. Zagorska, *Macromolecules* **1998**, *31*, 5051.
[55] A. Zen, P. Pingel, F. Jaiser, D. Neher, J. Grenzer, W. Zhuang, J. P. Rabe, A. Bilge, F. Galbrecht, B. S. Nehls, T. Farrell, U. Scherf, R. D. Abellón, F. C. Grozema, L. D. A. Siebbeles, *Chem. Mater.* **2007**, *19*, 1267.
[56] J. M. Warman, M. P. De Haas, A. Hummel, *Chem. Phys. Lett.* **1973**, *22*, 480.
[57] J. M. Warman, M. P. de Haas, G. Dicker, F. C. Grozema, J. Piris, M. G. Debije, *Chem. Mater.* **2004**, *16*, 4600.